Available online at www.sciencedirect.com
ScienceDirect
Journal of Solid State Chemistry 180 (2007) 1456–1463
JOURNAL OF SOLID STATE CHEMISTRY
www.elsevier.com/locate/jssc

Bi_2WO_6 photocatalytic films fabricated by layer-by-layer technique from Bi_2WO_6 nanoplates and its spectral selectivity

Shicheng Zhang[a,*], Jiandong Shen[a], Hongbo Fu[a], Weiyang Dong[a], Zhijian Zheng[a], Liyi Shi[b]

[a]*Department of Environmental Science & Engineering, Fudan University, Shanghai 200433, PR China*
[b]*Research Center of Nano-Science and Nano-Technology, Shanghai University, Shanghai 200444, PR China*

Received 3 December 2006; received in revised form 7 February 2007; accepted 18 February 2007
Available online 28 February 2007

Abstract

Bi_2WO_6 multilayer films have been fabricated successfully by a layer-by-layer (LbL) technique from Bi_2WO_6 nanoplates, which show higher visible-light photoactivity ($\lambda > 420$ nm) than that of Bi_2WO_6 nanoplate powders and P25 TiO_2 films. The films were characterized by X-ray diffraction (XRD), field emission scanning electron microscopy (FE-SEM), and UV–visible absorption spectroscopy. Photocatalytic activities of the films were evaluated by the rhodamine B (RhB) decomposition under UV and visible-light irradiation. Thickness and photoactivity of the film can be modified easily by changing the deposition cycles. Bi_2WO_6 films have the spectral selectivity of the photocatalytic degradation of RhB. Under the wavelength greater than 300 nm, the RhB molecules tend to be transformed to rhodamine over Bi_2WO_6 films selectively. However, in the case of shorter wavelength ($\lambda = 254$ nm) light irradiation, the RhB molecules can be photodegraded completely.

Keywords: Bi_2WO_6; Nanoplates; Layer-by-layer; Photocatalysis; Rhodamine B; Spectral selectivity

1. Introduction

Semiconductor photocatalysts have attracted great interests for their application in the environmental remediation, water splitting, the fixation of CO_2 and N_2, and the photosynthesis of organic compounds [1–3]. TiO_2 has by far the most popular one for its higher photocatalytic activity, good photostability, non-toxicity, and low price. But the large bandgap of TiO_2 (3.2 eV) makes it necessary for excitation only by UV light with wavelengths below 387 nm, which limits the usage efficiency of solar energy (max. 5%) and hinders the commercialization of this technology. Therefore, in order to eliminate the drawback, exploitation of new visible-light-driven photocatalysts has received considerable attention.

In recent years, Bi_2WO_6 has been demonstrated to be a good visible-light-driven photocatalysts. Kudo and Hijii [4] first demonstrated the photocatalytic O_2 evolution over Bi_2WO_6 from $AgNO_3$ solution. Subsequently, Tang et al. [5] reported that Bi_2WO_6 was also active for photocatalytic mineralizing both $CHCl_3$ and CH_3CHO. More recently, we successfully enhanced its photocatalytic activity by synthesizing nanostructured Bi_2WO_6, i.e. the nanoplates by hydrothermal process [6–8], and the nanoparticles by calcining amorphous complex precursor [9]. Yu et al. [10] also prepared the Bi_2WO_6 nanoparticles by hydrothermal method. Especially, Bi_2WO_6 nanoplates show higher activity, and have the potential use in environmental remediation induced by solar energy. Unfortunately, Bi_2WO_6 has a bigger molecular weight than that of TiO_2, and is more difficult to be dispersed in aqueous solution, which is a drawback for heterogeneous photocatalysis by photocatalysts dispersion [8]. For the photocatalytic reaction is a surface reaction, in order to eliminate the previous drawback, it is essential to expose the surface of Bi_2WO_6 nanoplates to the contaminants and the light. The Bi_2WO_6 films should be one of the best choices.

*Corresponding author. Fax: +86 21 6564 2080.
E-mail address: zhangsc@fudan.edu.cn (S. Zhang).

0022-4596/$ - see front matter © 2007 Elsevier Inc. All rights reserved.
doi:10.1016/j.jssc.2007.02.013

Hamada et al. [11] epitaxially deposited Bi_2WO_6 films on Nb-doped $SrTiO_3$ substrate by pulsed laser deposition, and investigated the dielectric properties. Ishikawa et al. [12] deposited Bi_2WO_6 films by metalorganic chemical vapor deposition, and investigated the ferroelectricity. Recently, we have fabricated the Bi_2WO_6 films from amorphous complex precursor, and investigated the photoelectric properties [13]. However, to the best of our knowledge, there are still no reports about photocatalytic activity of Bi_2WO_6 films.

Layer-by-layer (LbL) technique by sequential adsorption of oppositely charged materials (ranged from polyelectrolytes to inorganic materials) is one of the most promising ways of fabricating multilayer thin films with precisely controlled composition, thickness, and architecture on a nanometer scale [14–23]. Recently, some researchers reported the photocatalytic films fabricated by LbL technique [24–28]. But few reports are about the fabrication of multilayer films of complex oxide visible-light-driven photocatalysts.

Here, we reported the fabrication of Bi_2WO_6 films by sequential adsorption of Bi_2WO_6 nanosheets and polyelectrolytes, which showed higher photocatalytic activities under visible-light irradiation ($\lambda > 420$ nm). Thicknesses and photocatalytic activities of Bi_2WO_6 films were easily controlled by modifying the deposition layer numbers. The spectral selectivity of the rhodamine B (RhB) photodegradation on the surface of Bi_2WO_6 films was also discussed.

2. Experimental

2.1. Materials

Polyethylenimine (PEI), 50 wt% aqueous solutions, with molecular weight of 6×10^5, was purchased from Aldrich Co. and used without further purification. All solutions were prepared from deionized water. All other solvents and chemicals were of reagent grade. P25 TiO_2 (ca. 80% anatase, 20% rutile; BET area ca. $50\,m^2\,g^{-1}$) was kindly supplied by Degussa Co.

Bi_2WO_6 nanoplates were prepared by the hydrothermal synthesis according to the previous reports [6,7]. In a typical synthesis procedure, 5 mmol $Bi(NO_3)_2 \cdot 5H_2O$, 2.5 mmol H_2WO_4, and 5 mmol KOH were added to 35 mL deionized water with magnetic stirring. The mixture was sealed in a Teflon-lined stainless steel autoclave and heated at 180 °C for 24 h. After cooling, the resulting samples were collected and washed with deionized water and dried at 80 °C in air.

2.2. LbL assembly

Deposition of the Bi_2WO_6 films by LbL technique was carried by the similar procedure as reported in other related studies [20], which was described as follows.

Quartz substrates were cleaned by 3:7 (vol%) H_2O_2/H_2SO_4 (piranha solution) at 100 °C for ca. 40 min, followed by sonication in deionized water for 1 h, and then extensive rinsed with deionized water [29]. After cleaning, the substrates were negatively charged. Bi_2WO_6 nanoplates were dispersed in deionized water to yield a $2\,g\,L^{-1}$ suspension, and the pH of the suspension was adjusted to 10 by 1 M KOH solution to create a negatively charged surface for Bi_2WO_6 nanoplates.

Substrates were primed by being treated with a PEI solution ($2.5\,g\,L^{-1}$) to introduce the positive charge to the substrate surface. Primed substrates were dipped into Bi_2WO_6 nanoplates suspension to prepare a monolayer film by electrostatic deposition principle. Substrates and films were rinsed with water to remove the excessively adsorbed species and dried with air blow between the deposition steps. Repeating these layers produces n layers on the substrates.

As comparison, TiO_2 films were also prepared by the similar procedure. The TiO_2 (P25 TiO_2) suspension was $1\,g\,L^{-1}$, with the pH of 10.

2.3. Characterizations

XRD patterns were collected using a Rigaku Rint 2000S powder diffractometer with graphite monochromatized Cu$K\alpha$ radiation ($\lambda = 0.15405$ nm). The surface morphology of LbL films was observed by field emission scanning electron microscopy (FE-SEM; JEOL, JSM-6700F). UV–visible absorption spectra for monolayer and multilayer films fabricated on a quartz-glass substrate were recorded using a ThermoSpectronic UV500 UV–visible spectrometer.

2.4. Photochemical experiments

Photocatalytic activities of the films were evaluated by the RhB decomposition under UV and visible-light irradiation. UV light was obtained by a 25 W Hg lamp ($\lambda = 254$ nm) and the average light intensity was $400\,\mu W\,cm^{-2}$. A 500 W xenon lamp (Beijing TrusTech Science and Technology Co.) and different cutoff filters ($\lambda > 300$ nm, $\lambda > 350$ nm, and $\lambda > 420$ nm) were used to obtain the desired irradiation. The average light intensity was $100\,mW\,cm^{-2}$. The radiant flux was measured with a photometer (International Light Model IL1400A).

Bi_2WO_6 or TiO_2 films were dipped into the RhB solution (1×10^{-5} M, 50 mL) in a quartz vessel ($3 \times 3 \times 10\,cm^3$) vertically. The light was irradiated from side and perpendicular to the surface of the films. The size of the films was about $2.5 \times 2.5\,cm^2$. Air was bubbled into the reactor with a flow rate of $40\,mL\,min^{-1}$. At given time intervals, 1 mL aliquots were sampled, and analyzed by recording the variations of the absorption band maximum (554 nm) in the UV–visible spectrum of RhB using a ThermoSpectronic UV500 UV–visible spectrometer.

As comparison, the photodegradation of RhB by 1 mg of Bi_2WO_6 nanoplates, similar weight of Bi_2WO_6 on eight layers LbL film (about 0.6 ± 0.1 mg), was performed. RhB solutions (100 mL 10^{-5} mol L^{-1}) containing 1 mg of Bi_2WO_6 nanoplates was put in the same quartz vessel. Before the light was turned on, the solution was stirred for 30 min to ensure equilibrium between the catalyst and the solution. One milliliter of samples were taken at given time intervals and separated through centrifugation (10,000 rpm, 10 min). The supernatants were analyzed by recording variations of the absorption band maximum (554 nm).

3. Results and discussion

3.1. Fabrication of Bi_2WO_6 multilayer films

Scheme 1 schematically displays the overall procedure for the synthesis of Bi_2WO_6 multilayer films. Firstly, the surface of the quartzes was modified with PEI to be positively charged. Next, the negatively charged Bi_2WO_6 nanoplates were adsorbed onto the surface of these polymer templates to form composite films due to the electrostatic attraction between them. To fabricate thicker Bi_2WO_6 films, PEI and the Bi_2WO_6 nanosheets were alternatively deposited on quartzes for a specified number of cycles. Every deposition step involved dipping, rinsing, drying, and re-dipping operations.

There are many deposition parameters to be examined in the fabrication of a high-quality films. Because the adsorption of PEI has been examined and conditions to obtain its monolayer coverage have been established, most typical deposition parameters in the literatures were used as indicated in Experimental section. In this study, the adsorption behaviors of Bi_2WO_6 nanoplates were examined to obtain a deposited layer of densely titled nanoplates.

At a given concentration of PEI solution or Bi_2WO_6 nanoplates suspension, the dipping duration is an important factor for adsorption of PEI or Bi_2WO_6 nanoplates. Fig. 1 shows the UV–vis absorbance of the PEI/Bi_2WO_6 bilayer deposited on a quartz-glass substrate as a function of the dipping duration in PEI solution and Bi_2WO_6 nanoplates suspension. For the PEI molecular is relatively small, the adsorption of PEI molecular onto the surface of negative charged quartz-glass substrates is too rapid to saturated in a few minutes. However, the adsorption of the Bi_2WO_6 nanoplate "but not Bi_2WO_6 single molecule" onto the positive charged substrates was much slower for its bigger size. So there is a tendency for the absorbance to increase with the dipping duration in Bi_2WO_6 nanoplates suspension. Exceed to 60 min, no distinct increment was observed, suggesting a saturation of adsorption.

The multilayer buildup process was monitored with a UV–vis spectrum of the film after each deposition cycle as depicted in Fig. 2. The spectral profile has a peak at 250 nm. The higher baseline in the visible-light region is attributable to reflectance by the nanoplates on the film surface [27,30]. The polycation PEI does not have

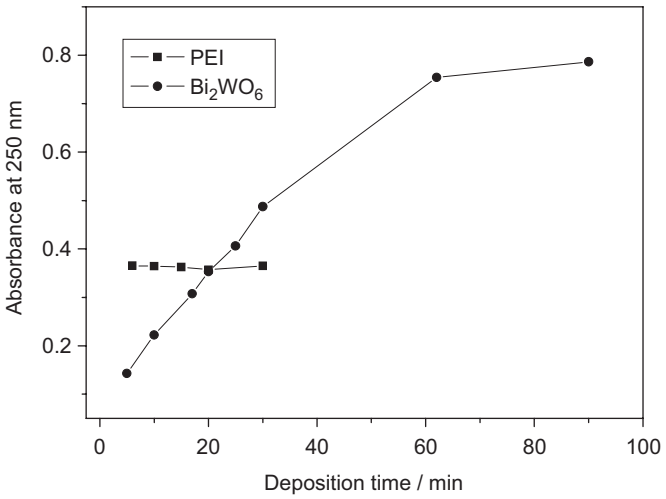

Fig. 1. Effects of duration time on absorbance for PEI and Bi_2WO_6.

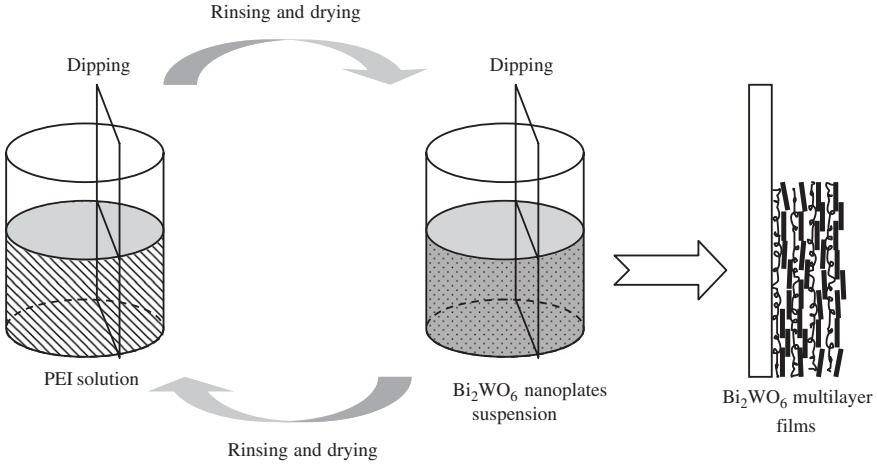

Scheme 1. Schematic illustration of the fabrication procedures for Bi_2WO_6 multilayer films.

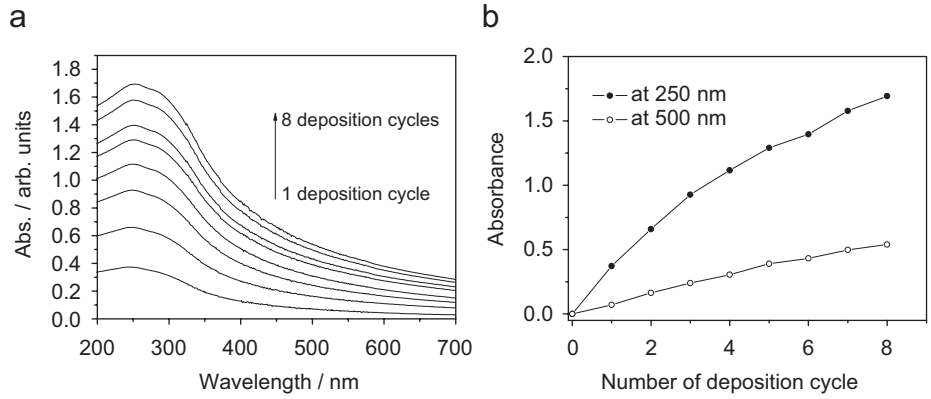

Fig. 2. (a) UV–is absorption spectra of Bi_2WO_6 films in the multilayer buildup process. (b) Absorbance at 250 and 500 nm vs. the deposited PEI/Bi_2WO_6 dilayers. Experimental conditions employed for this film growth: duration time of 20 min.

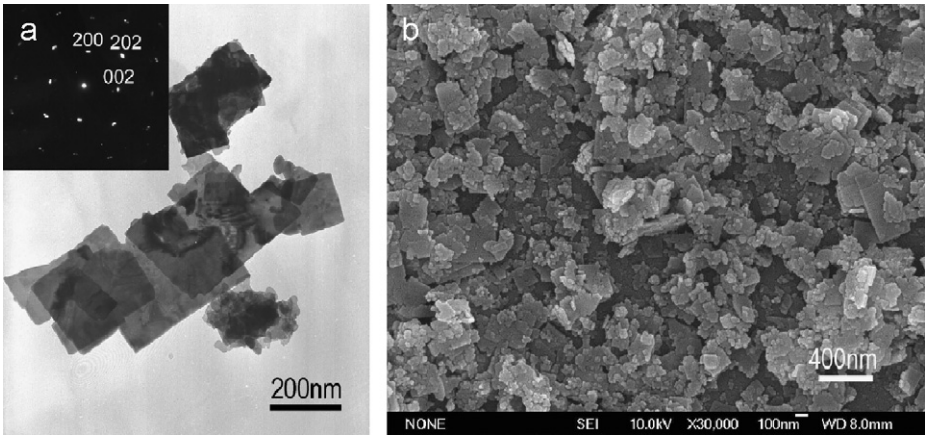

Fig. 3. (a) TEM image of Bi_2WO_6 nanoplates and the electron diffraction pattern (inset); (b) FE-SEM morphology of Bi_2WO_6 multilayer film with eight deposition layers.

absorption in this spectral range. Thus, a nearly linear enhancement in peak-top absorbance provides evidence for the regular growth of the multilayer assembly, and that the binding forces between the already deposited and the newer layers changes little increasing the layer number.

The film thickness was calculated by measuring the mass of the nanofilms and the surface area of the substrate glass slides [31]. The thickness values were calculated according to

$$= \frac{m}{\rho A} \times 10^4, \quad (1)$$

where d (nm), m (mg), ρ (g cm^{-3}) and A (cm^2) are the thickness, the mass, the mean density and the surface area of the deposited films, respectively. The mean density of the films is composed with the densities of the PEI molecular and the Bi_2WO_6 nanoplates. Because the exact mass ratio of PEI molecular and Bi_2WO_6 nanoplates was not clear, and there are some pores on the film, which could be seen from the FE-SEM (Fig. 3(b)), it is very difficult to get the exact mean density of the deposited films. In our calculations, the mean density was approximate to the density of Bi_2WO_6, and using macroscopic density of 9.505 g cm^{-3} for orthorhombic Bi_2WO_6, which was bigger than the exact one. Calculated thickness of Bi_2WO_6 films with eight deposition layers was 50 ± 8 nm, and the average thickness of one layer is 6 ± 1 nm. For the reason of the bigger mean density in calculation, the calculated thickness of the film should be smaller than the actual one.

Fig. 3 shows TEM image of Bi_2WO_6 nanoplates and the surface morphology of Bi_2WO_6 multilayer films. Bi_2WO_6 multilayer films present a dense surface with some pores. Most of Bi_2WO_6 nanoplates were flat lying on the surface, and their morphologies were similar to that from TEM images (Fig. 3(a)). The selective area electron diffraction (SAED) pattern of individual flat-lying nanoplates showed regular square diffraction spot array, corresponding to the lattice spacing of 0.273, 0.272 nm are from the (2 0 0), (0 0 2) Bragg reflection of the orthorhombic Bi_2WO_6, respectively. From the XRD patterns of Bi_2WO_6 multilayer films (Fig. 4), we can also find that the peaks of (0 2 0) and (0 6 0) were enhanced, and the peak of (1 3 1) was weakened, which suggests preferential orientation of the (0 2 0) face of Bi_2WO_6 parallel to the substrate. This

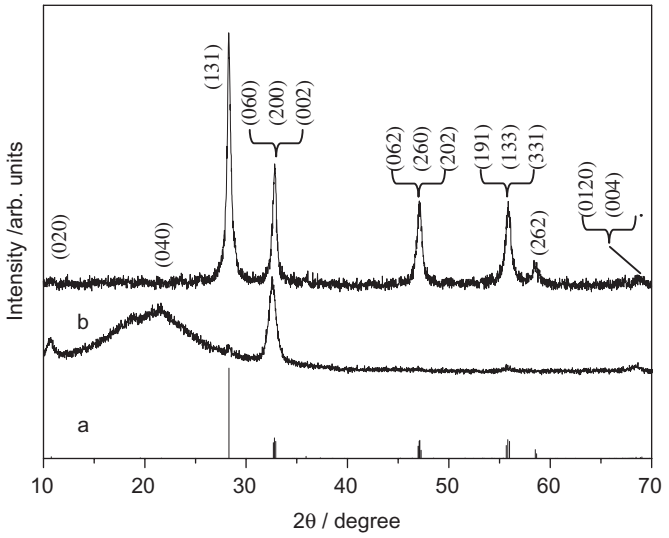

Fig. 4. XRD patterns of Bi_2WO_6 multilayer films prepared by LbL technique (b). Also show the standard patterns of orthorhombic Bi_2WO_6 (a, JCPDF 79-2381) and the XRD patterns of Bi_2WO_6 nanoplate powders (c).

implicated that most of the nanoplates were parallel to the substrate, which was similar to the FE-SEM results (Fig. 3).

3.2. Evaluation of photocatalytic activity

The photocatalytic activity of Bi_2WO_6 films was evaluated by the degradation of RhB molecules. Fig. 5(a) shows time profiles of $\ln[C/C_0]$ under visible-light irradiation ($\lambda > 420$ nm), where C was the concentration of RhB at the irradiation time t and C_0 was the concentration in the adsorption equilibrium on Bi_2WO_6 before irradiation. The $\ln[C/C_0]$ linearly decreased, which means the photodegradation of RhB over Bi_2WO_6 films could be described as apparent first-order reaction [6]. Fig. 5(b) shows the values of the photodegradation rate constant k vs. the duration time of the substrate in Bi_2WO_6 suspension. The photocatalytic activity of Bi_2WO_6 can be evaluated by the value of k, i.e. the bigger the value of k, the higher the photocatalytic activity. With the increase of the duration time, the photodegradation rate constant increased rapidly in the first 20 min, and increased slowly in the next 40 min and reached the maximum at 60 min. Subsequently, the photodegradation rate constant decreased. The phenomenon could be interpreted by Fig. 1. With the increase of duration time, the thickness of Bi_2WO_6 films increased firstly and then reached a plateau for the adsorption saturation. With the longer duration time (e.g. 90 min), though the thickness did not change obviously, the photodegradation rate constant decreased. So we choose the duration time of 20 min in our following experiment for the reasons of photocatalytic activity and time.

The photocatalytic activity of Bi_2WO_6 films with different thickness obtained by changing the deposition

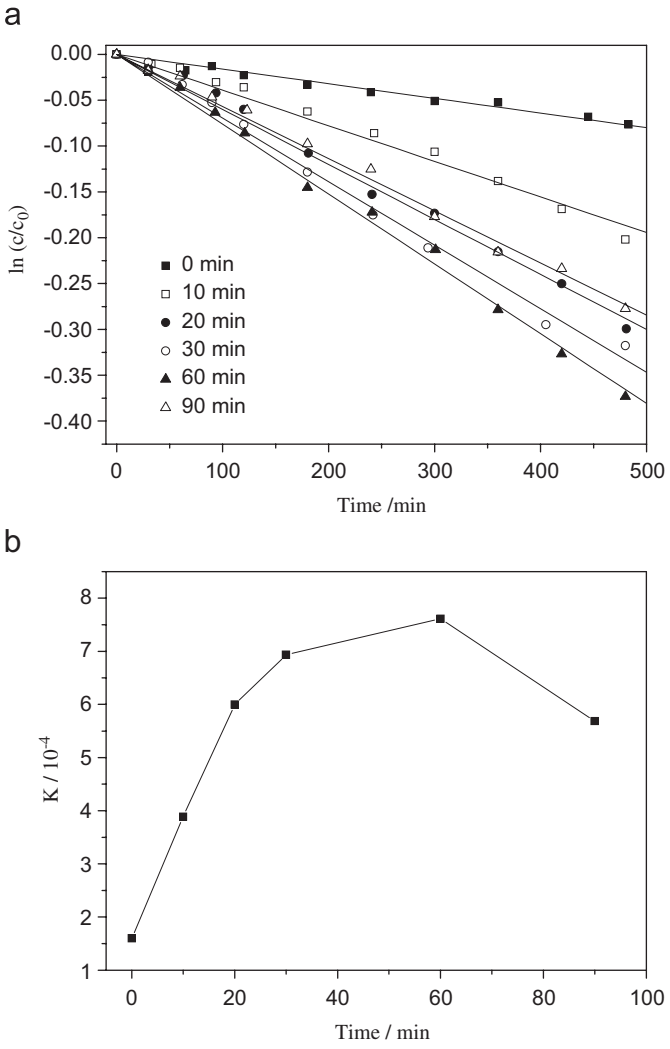

Fig. 5. Photocatalytic degradation of RhB (10^{-5} mol L^{-1}) under visible light ($\lambda > 420$ nm) at room temperature in air for 480 min over Bi_2WO_6 monolayer films prepared under different duration time in Bi_2WO_6 suspension: (a) time profile, (b) rate constant k vs. duration time.

cycles are shown in Fig. 6. We can find that all the photocatalytic reactions belong to apparent first-order reaction, and with the increase of deposition cycles, the reaction constant increases linearly. More than 90% of RhB can be photodegraded in 480 min over the eight deposition cycles Bi_2WO_6 films under visible-light irradiation ($\lambda > 420$ nm). For the amount of Bi_2WO_6 on the substrate with eight deposition cycles is only 0.6 ± 0.1 mg, it is possible to improve the photocatalytic activity by increasing the thickness.

Fig. 7 shows the comparison of photoactivity of Bi_2WO_6 multilayer films and Bi_2WO_6 nanoplate powders. For the amount of Bi_2WO_6 nanoplates on the film (0.6 ± 0.1 mg) and in powder form (1 mg) are similar, their photoactivity is comparable. Bi_2WO_6 nanoplates fixed on the substrates can absorb the light efficiently and have a higher photoactivity than that of Bi_2WO_6 nanoplate powders. So, Bi_2WO_6 multilayer film is an efficient strategy to

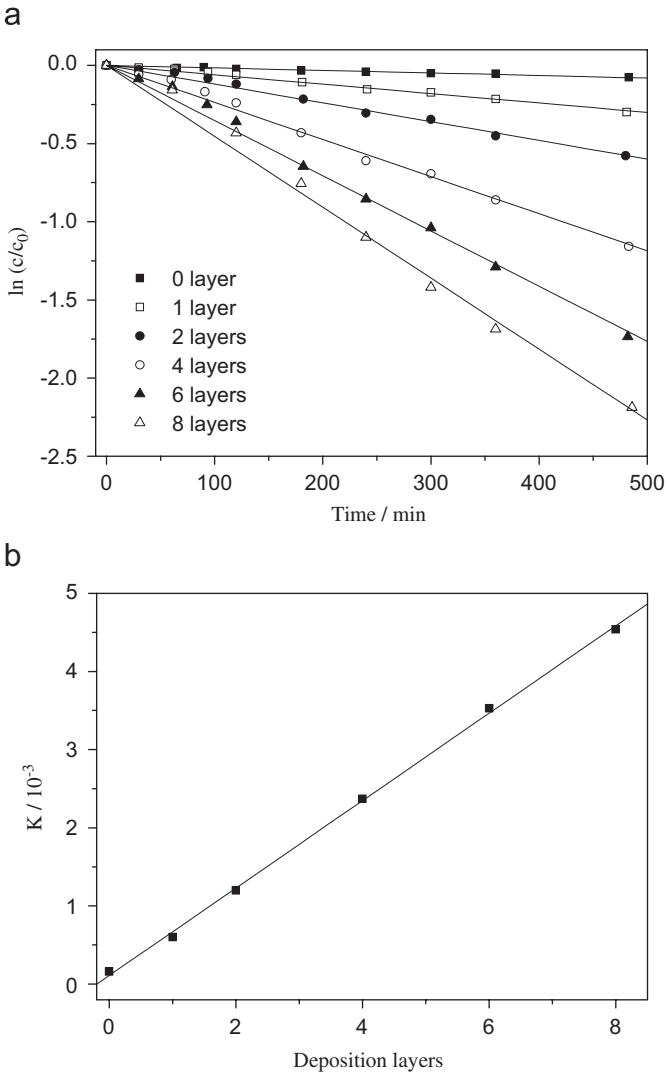

Fig. 6. Photocatalytic degradation of RhB (10^{-5} mol L^{-1}) under visible light ($\lambda > 420$ nm) at room temperature in air for 480 min over Bi_2WO_6 multilayer films with different layer number: (a) time profile, (b) rate constant k vs. layer number.

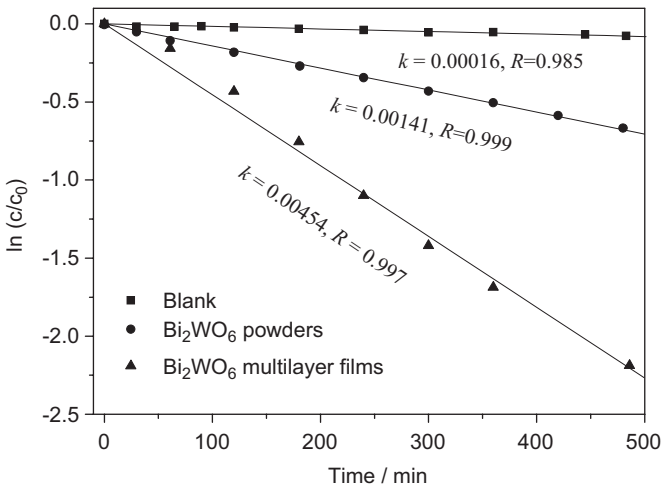

Fig. 7. Photocatalytic degradation of RhB (10^{-5} mol L^{-1}) under visible light ($\lambda > 420$ nm) at room temperature in air for 480 min over Bi_2WO_6 multilayer films (eight layers, 0.6 ± 0.1 mg) and Bi_2WO_6 nanoplate powders (1 mg). Also show the rate constants k and correlation coefficients R.

overcome the drawback of being difficult to be dispersed in aqueous solution for heterogeneous photocatalysis by Bi_2WO_6 nanoplate powders [8]. In addition, Bi_2WO_6 multilayer film is more convenient to separate from the solution after photocatalysis than that of Bi_2WO_6 nanoplate powders.

To further observe the photochemical property of Bi_2WO_6 films, the RhB photodegradation by Bi_2WO_6 films with eight deposition cycles was performed under the different irradiation wavelengths. By comparison, the RhB photodegradation by TiO_2 (P25) multilayer films with eight deposition cycles was also performed under the same conditions. The temporal evolutions of the spectral changes taking place during the RhB photodegradation are shown in Figs. 8 and 9.

Under the visible-light irradiation ($\lambda > 420$ nm), the RhB photodegradation by Bi_2WO_6 films is much faster than that by TiO_2 films (Figs. 8(a) and (b)). At the shorter wavelength, the photodegradation rate is faster for TiO_2 films. And during the photodegradation procedure, the changes of absorption spectra were different for the RhB/Bi_2WO_6 films system from that of the RhB/TiO_2 films system. Longer wavelength light irradiation ($\lambda > 300$ nm; Figs. 8(a)–(e)) of the aqueous RhB/Bi_2WO_6 films leads to a decrease in the absorption with a concomitant wavelength shift of the band to shorter wavelengths. However, the shorter wavelength light irradiation ($\lambda = 254$ nm; Fig. 9) leads to a repaid decrease in the absorption without the obvious wavelength hypsochromic shifts. In contrast, in the RhB/TiO_2 films system, all wavelength light irradiation leads to a rapid decrease in absorption (Figs. 8(b), (d) and 8(f)).

It was well reported that the RhB photodegradation occurs via two competitive process: *N*-demethylation and the destruction of the conjugated structure [32,33]. The wavelength hypsochromic shifts were attributed to the *N*-demethylation, and ultimately, the new absorbance band at 498 nm appeared, suggesting the fully de-ethylated RhB molecule (i.e. rhodamine) formed. The rapid decrease of absorption was mainly attributed to the destruction of the conjugated structure. As a result, the RhB photodegradation in RhB/Bi_2WO_6 films system, under the irradiation wavelength greater than 300 nm, was predominantly *N*-demethylation process, and the ultimate product was mainly rhodamine. For the wavelength of the sun light in troposphere is greater than 300 nm [34], the sun light irradiation of the aqueous RhB/Bi_2WO_6 films leads to formation of rhodamine, and cannot photodegrade the RhB molecules completely. This materials have the potential application in selective oxidation and photosynthesis under longer wavelength irradiation ($\lambda > 300$ nm).

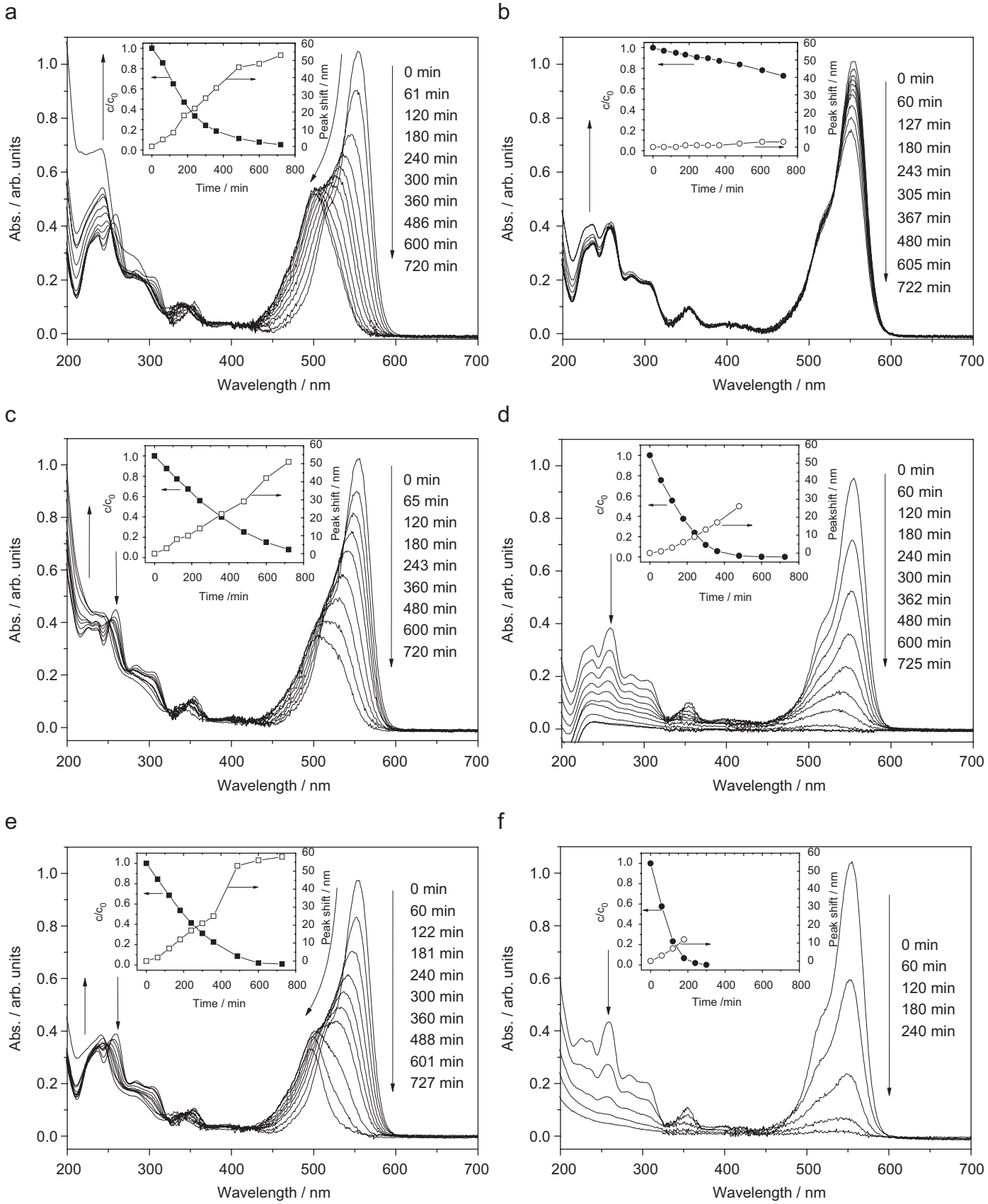

Fig. 8. Temporal UV–visible absorption spectral changes observed for the RhB solutions under different irradiation wavelengths for RhB/Bi_2WO_6 system (a, $\lambda > 420$ nm; c, $\lambda > 350$ nm; e, $\lambda > 300$ nm) and RhB/TiO_2 system (b, $\lambda > 420$ nm; d, $\lambda > 350$ nm; f, $\lambda > 300$ nm). Inset shows the changes of RhB concentration and the absorption peak shifts. The arrows show the changing direction of absorption spectra with the prolonging of irradiation time.

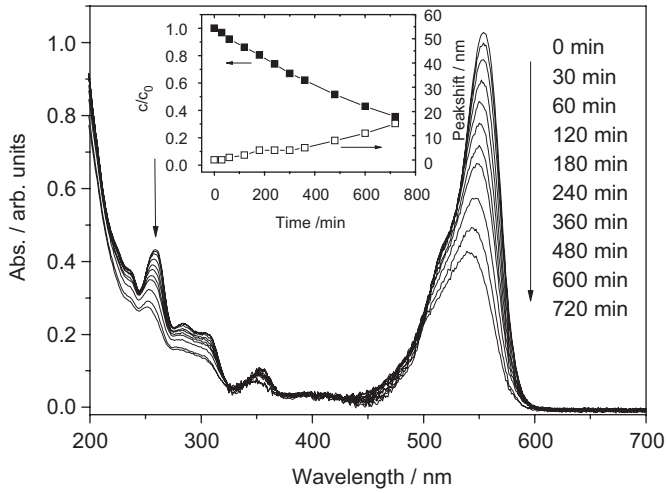

Fig. 9. Temporal UV–visible absorption spectral changes observed for the RhB solutions under UV light irradiation ($\lambda = 254$ nm) for RhB/Bi_2WO_6 system. Inset shows the changes of RhB concentration and the absorption peak shifts. The arrows show the changing direction of absorption spectra with the prolonging of irradiation time.

4. Conclusions

In summary, Bi_2WO_6 multilayer films have been fabricated successfully by a LbL technique from Bi_2WO_6 nanoplates, which showed higher visible-light photoactivity ($\lambda > 420$ nm) than that of Bi_2WO_6 nanoplate powders and P25 TiO_2 films. Thickness and photoactivity of the films can be modified easily by changing the deposition cycles. Bi_2WO_6 films have the spectral selectivity of the photocatalytic degradation of RhB. Under the wavelength greater than 300 nm, the RhB molecules tend to be transformed to rhodamine over Bi_2WO_6 films. However, under the shorter wavelength ($\lambda = 254$ nm) light irradiation, the RhB molecules can be photodegraded completely. Generally, the Bi_2WO_6 films have both the potential application in selective oxidation and photosynthesis, and in photodegradation of dyes by the different wavelength light irradiation.

Acknowledgments

This work was supported by the National Natural Science Foundation of China (Grant no. 50502022), Shanghai Nanotechnology Promotion Centre (05nm05019), and the 5th Century Star Program of Fudan University.

References

[1] M.R. Hoffmann, S.T. Martin, W. Choi, D.W. Bahnemannt, Chem. Rev. 95 (1995) 69.
[2] A.L. Linsebigler, G. Lu, J.T. Yates Jr., Chem. Rev. 95 (1995) 735.
[3] O. Carp, C.L. Huisman, A. Reller, Progr. Solid State Chem. 32 (2004) 33.
[4] A. Kudo, S. Hijii, Chem. Lett. (1999) 1103.
[5] J.W. Tang, Z.G. Zou, J.H. Ye, Catal. Lett. 92 (2004) 53.
[6] C. Zhang, Y.F. Zhu, Chem. Mater. 17 (2005) 3537.
[7] H.B. Fu, C.S. Pan, W.Q. Yao, Y.F. Zhu, J. Phys. Chem. B 109 (2005) 22432.
[8] H.B. Fu, L.W. Zhang, W.Q. Yao, Y.F. Zhu, Appl. Catal. B 66 (2006) 100.
[9] S.C. Zhang, C. Zhang, Y. Man, Y.F. Zhu, J. Solid State Chem. 179 (2006) 62.
[10] J.G. Yu, J.F. Xiong, B. Cheng, Y. Yu, J.B. Wang, J. Solid State Chem. 178 (2005) 1968.
[11] M. Hamada, H. Tabata, T. Kawai, Thin Solid Films 306 (1997) 6.
[12] K. Ishikawa, T. Watanabe, H. Funakubo, Thin Solid Films 392 (2001) 128.
[13] S.C. Zhang, W.Q. Yao, Y.F. Zhu, L.Y. Shi, Acta Phys.-Chim. Chin. 23 (2007) 111.
[14] G. Decher, Science 277 (1997) 1232.
[15] S.C. Zhang, J. Chen, X.G. Li, Nanotechnology 15 (2004) 477.
[16] N. Sakai, G.K. Prasad, Y. Ebina, K. Takada, T. Sasaki, Chem. Mater. 18 (2006) 3596.
[17] K. Izawa, T. Yamada, U. Unal, S. Ida, O. Altuntasoglu, M. Koinuma, Y. Matsumoto, J. Phys. Chem. B 110 (2006) 4645.
[18] L. Wang, Y. Ebina, K. Takada, T. Sasaki, J. Phys. Chem. B 108 (2004) 4283.
[19] Z.S. Wang, T. Sasaki, M. Muramatsu, Y. Ebina, T. Tanaka, L.Z. Wang, M. Watanabe, Chem. Mater. 15 (2003) 807.
[20] L. Wang, T. Sasaki, Y. Ebina, K. Kurashima, M. Watanabe, Chem. Mater. 14 (2002) 4827.
[21] T. Sasaki, Y. Ebina, K. Fukuda, T. Tanaka, M. Harada, M. Watanabe, Chem. Mater. 14 (2002) 3524.
[22] T. Sasaki, Y. Ebina, T. Tanaka, M. Harada, M. Watanabe, G. Decher, Chem. Mater. 13 (2001) 4661.
[23] R.Z. Ma, T. Sasaki, Y. Bando, J. Am. Chem. Soc. 126 (2004) 10382.
[24] T.H. Kim, B.H. Sohn, Appl. Surf. Sci. 201 (2002) 109.
[25] M. Harada, T. Sasaki, Y. Ebina, M. Watanabe, J. Photochem. Photobio. A 148 (2002) 273.
[26] T. Szabo, J. Nemeth, I. Dekany, Colloid. Surf. A 230 (2003) 23.
[27] R. Kun, M. Balazs, I. Dekany, Colloid. Surf. A 265 (2005) 155.
[28] J.H. Kim, S. Fujita, S. Shiratori, Thin Solid Films 499 (2006) 83.
[29] H. Chen, G.H. Zeng, Z.Q. Wang, X. Zhang, M.L. Peng, L.Z. Wu, C.H. Tung, Chem. Mater. 17 (2005) 6679.
[30] Y.P. Sun, E.C. Hao, X. Zhang, B. Yang, J.C. Shen, L.F. Chi, H. Fuchs, Langmuir 13 (1997) 5168–5174.
[31] T. Szabo, J. Nemeth, I. Dekany, Colloid. Surf. A 230 (2003) 23.
[32] T.X. Wu, G.M. Liu, J.C. Zhao, H. Hidaka, N. Serpone, J. Phys. Chem. B 102 (1998) 5845.
[33] P. Qu, J.C. Zhao, T. Shen, H. Hidaka, J. Mol. Catal. A 129 (1998) 257.
[34] J.H. Seinfeld, S.N. Pandis, Atmospheric Chemistry and Physics, Wiley Inc., New York, 1998.